

Measurement of the $K_S \rightarrow \gamma\gamma$ branching ratio using a pure K_S beam with the KLOE detector

The KLOE Collaboration:

*F. Ambrosino^{c,d}, A. Antonelli^a, M. Antonelli^a, F. Archilli^a, P. Beltrame^b,
G. Bencivenni^a, S. Bertolucci^a, C. Bini^{f,g}, C. Bloise^a, S. Bocchetta^{h,i}, F. Bossi^a,
P. Branchiniⁱ, P. Campana^a, G. Capon^a, T. Capussela^a, F. Ceradini^{h,i}, F. Cesario^{h,i},
P. Ciambrone^a, F. Crucianelli^f, S. Conetti^l, E. De Lucia^a, A. De Santis^{f,g},
P. De Simone^a, G. De Zorzi^{f,g}, A. Denig^b, A. Di Domenico^{f,g}, C. Di Donato^d,
B. Di Micco^{h,i}, M. Dreucci^a, G. Felici^a, M. L. Ferrer^a, S. Fiore^{f,g}, P. Franzini^{f,g},
C. Gatti^a, P. Gauzzi^{f,g}, S. Giovannella^a, E. Grazianiⁱ, W. Kluge^b, V. Kulikov^k,
G. Lanfranchi^a, J. Lee-Franzini^{a,j}, D. Leone^b, M. Martini^{a*}, P. Massarotti^{c,d},
S. Meola^{c,d}, S. Miscetti^{a†}, M. Moulson^a, S. Müller^a, F. Murtas^a, M. Napolitano^{c,d},
F. Nguyen^{h,i}, M. Palutan^a, E. Pasqualucci^g, A. Passeriⁱ, V. Patera^{a,e}, F. Perfetto^{c,d},
P. Santangelo^a, B. Sciascia^a, A. Sciubba^{a,e}, A. Sibidanov^a, T. Spadaro^a, M. Testa^{f,g},
L. Tortoraⁱ, P. Valente^g, G. Venanzoni^a, R. Versaci^a.*

^aLaboratori Nazionali di Frascati dell'INFN, Frascati, Italy

^bInstitut für Experimentelle Kernphysik, Universität Karlsruhe, Germany

^cDipartimento di Scienze Fisiche dell'Università "Federico II", Napoli, Italy

^dINFN Sezione di Napoli, Napoli, Italy

^eDipartimento di Energetica dell'Università "La Sapienza", Roma, Italy

^fDipartimento di Fisica dell'Università "La Sapienza", Roma, Italy

^gINFN Sezione di Roma, Roma, Italy

^hDipartimento di Fisica dell'Università "Roma Tre", Roma, Italy

ⁱINFN Sezione di Roma Tre, Roma, Italy

^jPhysics Department, State University of New York at Stony Brook, USA

^kInstitute for Theoretical and Experimental Physics, Moscow, Russia.

^lPhysics Department, University of Virginia, USA.

ABSTRACT: We have searched for the decay $K_S \rightarrow \gamma\gamma$ in a sample of $\sim 2 \times 10^9$ $\phi \rightarrow K_S K_L$ decays collected at DAΦNE with an integrated luminosity of 1.9 fb^{-1} . K_S are tagged by the K_L interaction in the calorimeter. Two prompt photons must also be detected. Kinematic constraints reduce the initial 6×10^5 events to 2740 candidates, from which a signal of 711 ± 35 events is extracted. By normalizing to the $K_S \rightarrow 2\pi^0$ decays counted in the same sample, we measure $\text{BR}(K_S \rightarrow \gamma\gamma) = (2.26 \pm 0.12_{\text{stat}} \pm 0.06_{\text{syst}}) \times 10^{-6}$, in agreement with $\mathcal{O}(p^4)$ Chiral Perturbation Theory predictions.

KEYWORDS: e^+e^- collisions, DAΦNE, KLOE, rare K_S decays, χ PT.

Contents

1. Introduction	1
2. The KLOE detector	2
3. Search of $K_S \rightarrow \gamma\gamma$ with a pure K_S beam	2
3.1 K_S tagging and event preselection	2
3.2 Kinematic fitting and event counting	4
4. Branching ratio evaluation and systematics	7
5. Conclusion	11
6. Acknowledgements	12

1. Introduction

A precise measurement of the $K_S \rightarrow \gamma\gamma$ decay rate provides a test of Chiral Perturbation Theory (χPT). The $K_S \rightarrow \gamma\gamma$ decay amplitude has been evaluated at leading order of χPT , $\mathcal{O}(p^4)$, providing an estimate to a few percent accuracy of branching ratio, BR, $\text{BR}(K_S \rightarrow \gamma\gamma) = 2.1 \times 10^{-6}$ [1]. Measurement of such a BR has considerably changed with the time [2, 3] while improving the precision. The latest determination comes from NA48 [4], which gives a BR of $(2.71 \pm 0.07) \times 10^{-6}$. This result differs by about 30% from χPT $\mathcal{O}(p^4)$ prediction, suggesting possible contributions from higher order corrections.

We report a measurement based on a data sample of 1.9 fb^{-1} of e^+e^- collisions collected with the KLOE detector [5] at DAΦNE [6], the Frascati ϕ -factory. DAΦNE is an e^+e^- collider which operates at a center of mass energy, W , of $\sim 1020 \text{ MeV}$, the mass of the ϕ -meson. Equal-energy positron and electron beams collide at an angle of $(\pi - 25) \text{ mrad}$, producing ϕ -mesons nearly at rest. ϕ -mesons decay 34% of the time into nearly collinear $K^0\bar{K}^0$ pairs. Since $J^{PC}(\phi) = 1^{--}$, these pairs are in an antisymmetric state, so that the final state is always $K_S K_L$. This implies that detection of a K_L guarantees the presence of a K_S of given momentum and direction. We can thus identify K_S -mesons independently of the decay mode. We refer to this technique as tagging. The analyzed data sample corresponds to the production of ~ 2 billions of $K_S K_L$ pairs.

*Corresponding author. Email address: matteo.martini@lnf.infn.it

†Corresponding author. Email address: stefano.miscetti@lnf.infn.it

2. The KLOE detector

The KLOE detector consists of a large cylindrical drift chamber, DC [7], of 4 m diameter and 3.3 m length filled with a helium-based gas mixture, surrounded by a lead-scintillating fiber calorimeter, EMC [8]. A superconducting coil around the EMC provides a 0.52 T magnetic field. The low-beta insertion quadrupoles are inside the apparatus and are surrounded by two compact tile calorimeters with veto purposes, QCAL [9]. In this analysis, only the calorimeter system is used.

The EMC is divided into a barrel and two endcaps covering 98% of the solid angle. Modules are read out at both ends by photomultipliers, PM, with a $\sim (4.4 \times 4.4)$ cm² read-out granularity, for a total of 2440 cells. Both amplitude and time information are obtained from the PMs. The signal amplitude measures the energy deposited in the modules and its time provides both the arrival time of particles and the position along the modules of the energy deposits. Cells close in time and space are grouped into a “calorimeter cluster”. The cluster energy E is the sum of the cell energies. The cluster time T and position \vec{R} are energy-weighted averages. Energy and time resolutions are $\sigma_E/E = 5.7\%/\sqrt{E \text{ (GeV)}}$ and $\sigma_t = 57 \text{ ps}/\sqrt{E \text{ (GeV)}} \oplus 100 \text{ ps}$, respectively. The photon detection efficiency is $\sim 90\%$ at $E = 20 \text{ MeV}$ and reaches 100% above 70 MeV.

The QCAL is made of two tile calorimeters, $\sim 5 X_0$ thick, surrounding the two sets of low-beta quadrupoles. The coverage in polar angle is $0.94 < |\cos \theta| < 0.99$. Each calorimeter consists of a sampling structure of lead and scintillator tiles arranged in 16 azimuthal sectors. The readout is by wavelength shifter fibers coupled to mesh photomultipliers. The fiber arrangement allows the measurement of the longitudinal coordinate by time differences.

Calorimeter signals are used for the trigger [10]. Two energy deposits with $E > 50 \text{ MeV}$ for the barrel and $E > 150 \text{ MeV}$ for the endcaps are required. Identification and rejection of cosmic-ray events are also performed at the trigger level.

A background identification algorithm, Filfo [11], mainly based on calorimeter clustering runs offline over all collected data to reject residual cosmic-ray, machine background and Bhabha events fragmenting on QCAL before running the whole reconstruction program.

3. Search of $K_S \rightarrow \gamma\gamma$ with a pure K_S beam

3.1 K_S tagging and event preselection

The mean decay lengths in KLOE of the K_S and K_L are $\lambda_S \sim 0.6 \text{ cm}$ and $\lambda_L \sim 340 \text{ cm}$ respectively. About 50% of K_L 's reach the calorimeter before decaying. K_S 's are tagged with high efficiency ($\sim 30\%$) by identifying a K_L interaction, which we call K_L -crash. A K_L -crash has a very distinctive signature in the calorimeter, given by a late ($\beta_K = 0.2$) high-energy cluster not associated to any track. The K_L -crash provides a clean K_S tag. The average value of the center of mass energy, W , is obtained with a precision of 30 keV for each 100 nb^{-1} of data, by reconstructing large angle Bhabha scattering events. The mean interaction point, IP, position and momentum p_ϕ are also computed. The value of W , p_ϕ and the K_L -crash cluster position provide, for each event, the trajectory of the K_S

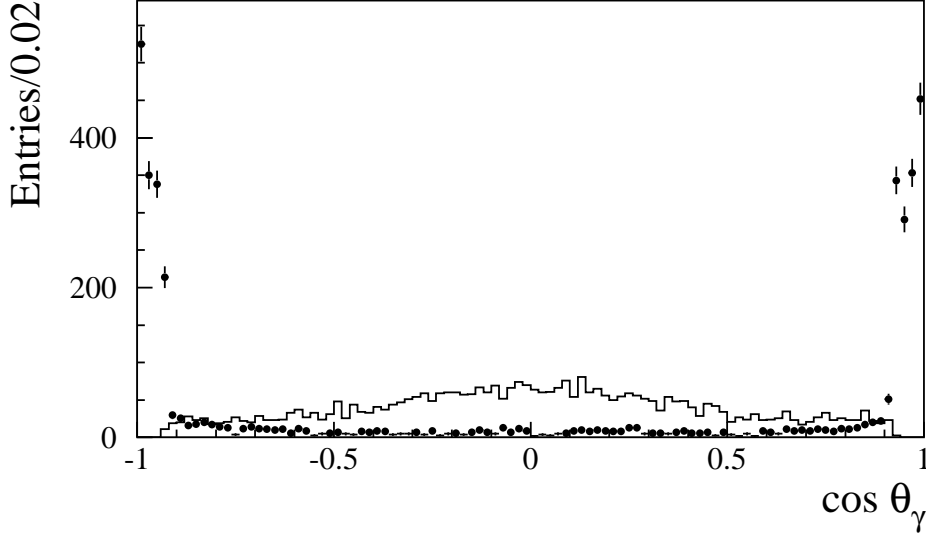


Figure 1: Angular distribution of photons for $K_S \rightarrow 2\pi^0$ MC events tagged by K_L -crash with two prompt photons in the EMC. Photons reconstructed by the EMC (solid-line), undetected photons (points).

with an angular resolution of 1° and a momentum resolution better than 2 MeV. In the analyzed sample of 1.9 fb^{-1} , we observe $\sim 700 \times 10^6$ K_S tagged events. Using the most recent value of $\text{BR}(K_S \rightarrow \gamma\gamma)$, we expect ~ 1900 tagged $K_S \rightarrow \gamma\gamma$ events.

Because of tagging, we have no $K_L \rightarrow \gamma\gamma$ background, the major contamination in the NA48 measurement. The main background in our analysis is due to $K_S \rightarrow 2\pi^0$ events with two undetected photons because out of acceptance or not reconstructed in the calorimeter.

We estimate background with the KLOE Monte Carlo, MC, [11], using a production of inclusive ϕ decays corresponding to an integrated luminosity of $\sim 1.5 \text{ fb}^{-1}$. In addition, for the signal we rely on a very large sample of MC $K_S \rightarrow \gamma\gamma$ events, equivalent to $\sim 100 \text{ fb}^{-1}$. In the simulation, the photon detection efficiency and resolutions have been tuned with data using a large sample of tagged photons in $\phi \rightarrow \pi^+\pi^-\pi^0$ events selected using only drift chamber information [11]. The interaction of the K_L in the main calorimeter is properly simulated.

The K_S decay length is negligible, then we assume that K_S decay photons propagate with $\beta = 1$ from the IP. A prompt photon is defined as a neutral cluster in the EMC, satisfying the condition $|T - R/c| < \min(5\sigma_t, 2\text{ns})$, where σ_t is the total time resolution. After tagging, we define a signal-enriched sample by requiring two prompt photons in the event. To improve the rejection of the main background, $K_S \rightarrow 2\pi^0$, we accept clusters with a low energy threshold, 7 MeV, produced in a wide angular acceptance, $|\cos(\theta)| < 0.93$.

After these acceptance cuts, we have a signal efficiency of $\sim 83\%$ and we count 550×10^3 events with a signal over background ratio, S/B, of $\sim 1/120$. The background composition is dominated by $K_S \rightarrow 2\pi^0$ events (99.1%) with a 0.7% residual contamination of fake K_L -crash from K^+K^- events, and an even smaller contamination of K_S decay channels

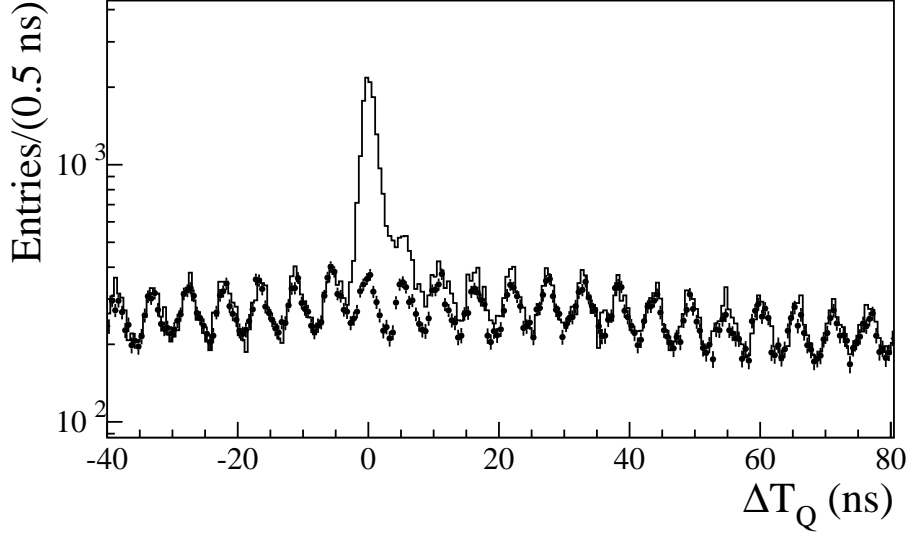


Figure 2: Inclusive distribution of the difference between the measured arrival time and the expected time of flight of hits in QCAL for events tagged by a K_L -crash with two prompt photons (solid line) or with a reconstructed $K_S \rightarrow \pi^+\pi^-$ decay (points).

different from $2\pi^0$ (0.2% $\pi^+\pi^-$, 0.02% $\pi l\nu$). The distribution of the photons not detected by the EMC for the background is peaked in the forward direction, as shown by the MC spectrum in Fig. 1.

To improve background rejection, we veto events with photons reaching QCAL. Fig. 2 shows the distribution of the difference between the reconstructed and the expected time of the QCAL hits, ΔT_Q . The sharp in-time peak is due to $K_S \rightarrow 2\pi^0$ with photons impinging on QCAL. The underlying distribution comes from machine background events and shows the period of the beam bunches. All events having at least one hit in QCAL with energy above the pedestal and in a time window, TW, defined by $|\Delta T_Q| < 5$ ns are vetoed. This cut rejects $\sim 70\%$ of the background, while retaining the signal with very high efficiency ($\sim 99.96\%$).

We should correct for the signal losses due to the accidental coincidence of machine background hits in the TW. A data-calibrated correction is evaluated as $C_Q = 1 - P_Q^{TW}$, where P_Q^{TW} is the probability of a random hit in TW. This has been estimated by averaging the results obtained in two different out-of-time windows, early and late with respect to the collision time. To estimate the systematic error, we determine P_Q^{TW} with reconstructed $K_S \rightarrow \pi^+\pi^-$ decays where no photons are present. We obtain: $P_Q^{TW} = (3.51 \pm 0.04_{\text{stat}} \pm 0.26_{\text{syst}})\%$.

At the end of the acceptance and QCAL veto selection, we remain with 157×10^3 events. The S/B is $\sim 1/120$ at this stage.

3.2 Kinematic fitting and event counting

To improve the S/B, we perform a kinematic fit with seven constraints: ϕ 4-momentum,

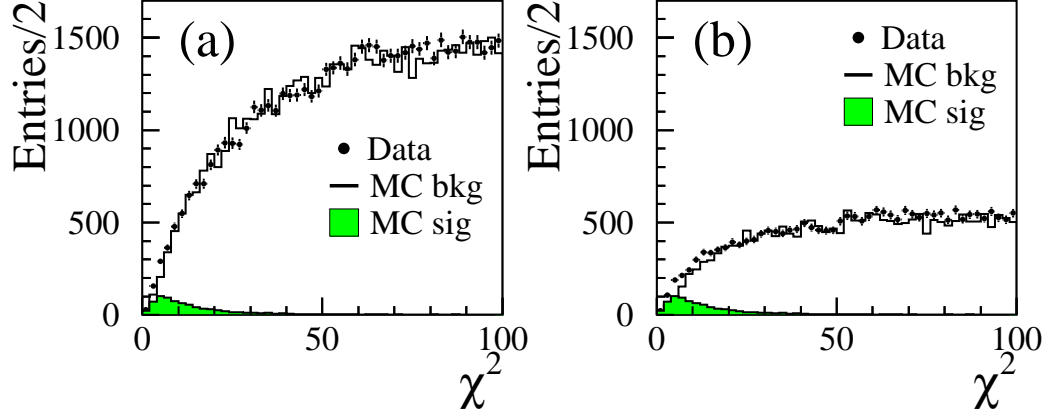


Figure 3: χ^2 distributions for tagged K_S events with two prompt photons: before (a) and after (b) QCAL veto.

kaon mass and the velocity for the two photons. Fig. 3 shows the χ^2 distribution from the fit for data and MC after the acceptance selection before and after the application of the QCAL veto. The background has high χ^2 values. Cutting at $\chi^2 < 20$ we retain $\sim 63\%$ of the signal while considerably reducing the background. The S/B improves from 1/120 to 1/3. After this cut, the background is entirely due to $K_S \rightarrow 2\pi^0$ events with two undetected photons.

Background can be further reduced using the $\gamma\gamma$ invariant mass, $M_{\gamma\gamma}$, and the photon opening angle in the kaon rest frame, $\theta_{\gamma\gamma}^*$. Since the kinematic fit imposes fixed values for the $K_S - K_L$ direction and the kaon mass, we use the reconstructed variables before fit constraining. In Fig. 4 the plot of $M_{\gamma\gamma}$ as a function of $\cos\theta_{\gamma\gamma}^*$ is shown for data and for MC background and signal.

To check the calorimeter description in the simulation, a data-MC comparison of response and resolution as a function of the incident photon energy is carried out by looking at the energy pulls of the kinematic fit for $K_S \rightarrow 2\pi^0$ events. $\sim 80 \text{ pb}^{-1}$ of Data and MC are used, tagged by K_L -crash and selected requiring four prompt photons. An energy scale correction is applied to better match simulation and data. After applying this correction, the MC ability in reproducing the signal shapes is tested with a control sample of $K_L \rightarrow \gamma\gamma$ events decaying near the beam pipe, tagged by a well reconstructed $K_S \rightarrow \pi^+\pi^-$ decay. 200 (450) pb^{-1} of data (MC) are used. A kinematic fit, similar to the one of the $K_S \rightarrow \gamma\gamma$ sample, is performed. The background is reduced to a negligible quantity cutting at $\chi^2(K_L) < 20$. A gaussian fit to the $M_{\gamma\gamma}$ distributions is shown in Fig. 5. The data and MC energy scales agree to better than 0.2%. The resolutions agree at a 0.5% level. The same control sample is also used to compare the $\chi^2(K_L)$ and $\cos\theta_{\gamma\gamma}^*(K_L)$ distributions which well match the simulated shape as shown in Fig. 6.

After the χ^2 cut, we count events in the K_S tagged sample by fitting with a binned maximum-likelihood the data distribution of $M_{\gamma\gamma} - \cos\theta_{\gamma\gamma}^*$. The likelihood function uses the

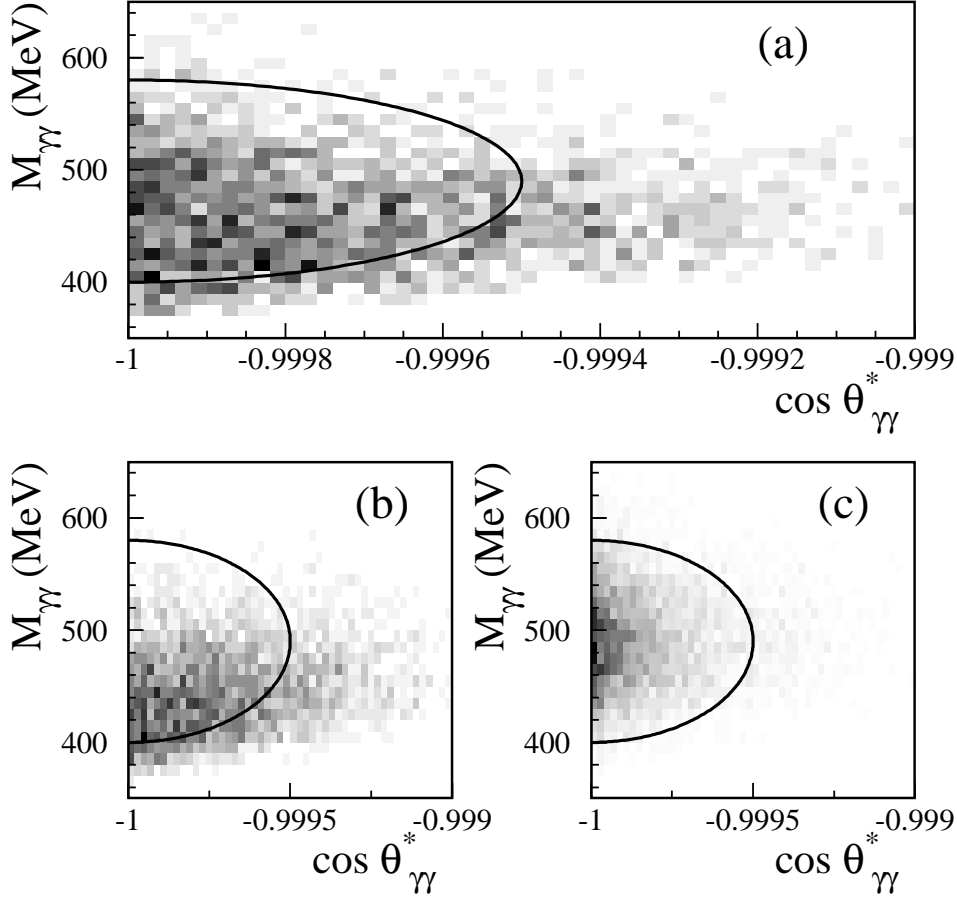


Figure 4: Scatter plot of $M_{\gamma\gamma}$ vs $\cos \theta_{\gamma\gamma}^*$ after pre-selection for data sample (a), Monte Carlo background (b) and signal (c). The solid curve represents the signal dominated region.

MC signal and background shapes and properly takes into account data and MC statistics. The fit gives $N(\gamma\gamma) = 711 \pm 35$, with a $\chi^2/\text{dof} = 854/826$, which corresponds to a $P(\chi^2)$ of 24%. The fit projections are shown in Fig. 7. As expected, the $\cos \theta_{\gamma\gamma}^*$ distribution for signal is more peaked than the background to -1 . The $M_{\gamma\gamma}$ signal distribution has a gaussian shape around the K_S mass, while the background shows an asymmetric shape peaked at lower mass values.

As an independent check of the fit quality, we show in Fig. 8.a the χ^2 distribution for data and MC after minimization. A similar comparison is done also for the angular photon spectrum (Fig. 8.b), which clearly indicates the presence of a flat component due to signal, as expected by the two body decay of a spin 0 particle.

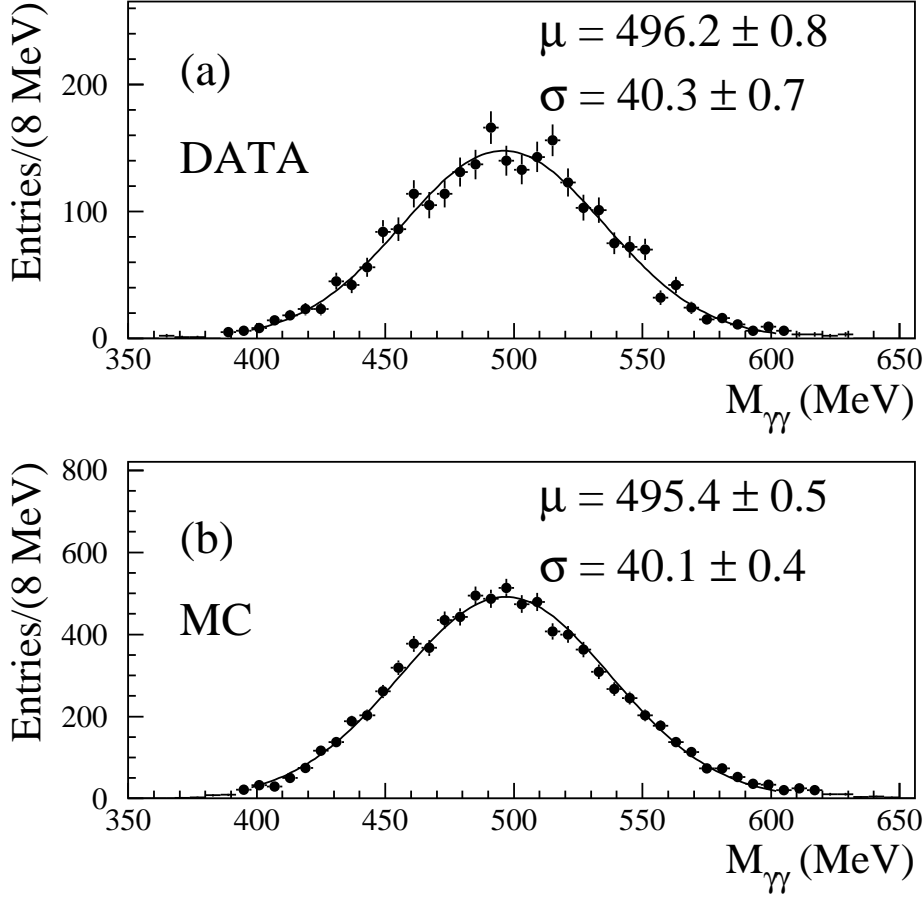


Figure 5: Distribution of the invariant mass of two photons for the $K_L \rightarrow \gamma\gamma$ control sample with a decay vertex near the beam pipe.

4. Branching ratio evaluation and systematics

The branching ratio is evaluated with respect to the $\text{BR}(K_S \rightarrow 2\pi^0)$ by normalizing the signal events, $N(\gamma\gamma)$, to the events with four prompt photons, $N(2\pi^0)$, counted in the same sample of K_L -crash events:

$$\text{BR}(K_S \rightarrow 2\gamma) = \frac{N(\gamma\gamma)}{N(2\pi^0)} \times \frac{\epsilon_{\text{TOT}}(2\pi^0|\text{tag})}{\epsilon_{\text{TOT}}(\gamma\gamma|\text{tag})} \times \text{BR}(K_S \rightarrow 2\pi^0) \times R_\epsilon \quad (4.1)$$

The total efficiencies have been evaluated by MC after K_L -crash tag. The signal total efficiency is the product of the efficiencies for the acceptance selection, the QCAL cut and the χ^2 cut:

$$\epsilon_{\text{TOT}}(\gamma\gamma) = \epsilon_{\text{sel}}(\gamma\gamma) \times \epsilon_{\text{Q}}(\gamma\gamma) \times \epsilon_{\chi^2}(\gamma\gamma). \quad (4.2)$$

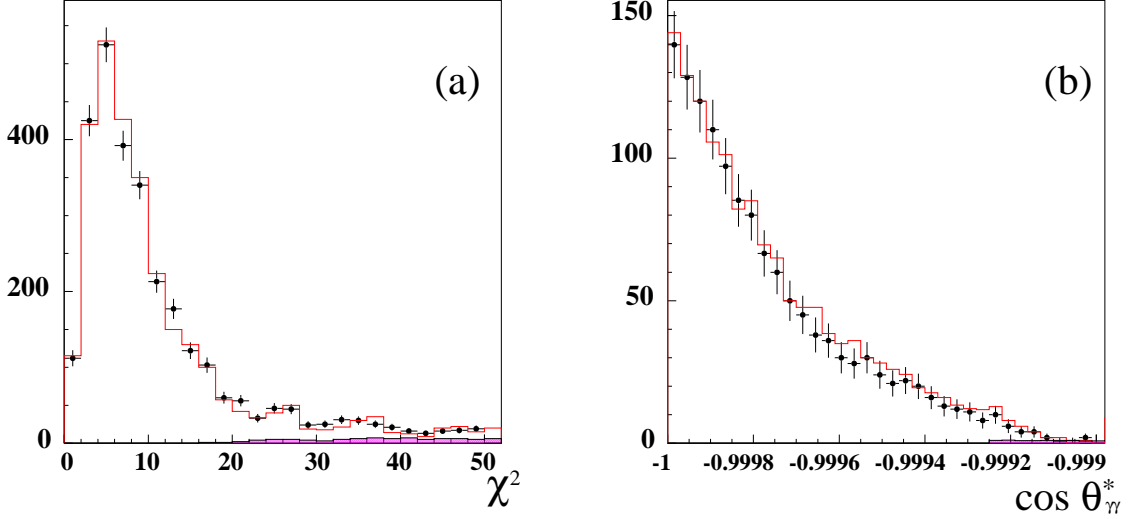


Figure 6: Distributions of χ^2 (a) and $\cos \theta_{\gamma\gamma}^*$ (b) for the $K_L \rightarrow \gamma\gamma$ control sample with a decay vertex near the beam pipe. Black points are data, solid line is MC.

For the normalization sample, the efficiency is related only to the acceptance of four photons. The ratio, R_ϵ , of all other efficiencies (triggering, Filfo filter and tagging) between signal and normalization sample is consistent with one. We get $R_\epsilon = 1.0003 \pm 0.0003_{\text{stat}}$. The difference from unity is added as contribution to the systematic error on the BR.

For the signal selection efficiency we find:

$$\epsilon_{\text{sel}}(\gamma\gamma) = (82.9 \pm 0.2_{\text{stat}} \pm 0.2_{\text{syst}})\%. \quad (4.3)$$

The large selection efficiency is due to the wide angular coverage of the calorimeter, the low energy threshold used and the almost flat angular distribution of the decay products. The systematic error assigned to this efficiency has been found by varying the data-MC correction of the cluster reconstruction efficiency. The efficiency for the QCAL cut is found from MC to be $\epsilon_Q^{MC}(2\gamma) \sim 99.96\%$. Applying the correction due to accidental losses described in sec. 3.1 we obtain:

$$\epsilon_Q(2\gamma) = \epsilon_Q^{MC}(2\gamma) \times C_Q = (96.45 \pm 0.04_{\text{stat}} \pm 0.26_{\text{syst}})\%. \quad (4.4)$$

The MC efficiency of the χ^2 cut is $\epsilon_{\chi^2} = (63.3 \pm 0.7)\%$. The systematic error related to the knowledge of the data-MC difference in the χ^2 scale has been evaluated by using the $K_L \rightarrow \gamma\gamma$ control sample. For the chosen χ^2 cut, we evaluate the data over MC ratio, R_c , of the χ^2 cumulative distributions and we get $(R_c - 1) = (-0.5 \pm 1.8)\%$. We conservatively assign the error on R as the contribution of the χ^2 scale to the systematic error.

The systematic uncertainties connected to the signal counting have been evaluated by repeating the analysis and the fit in different ways. The most delicate point is related to the simulation of the background shape. The MC shows a good agreement with data for

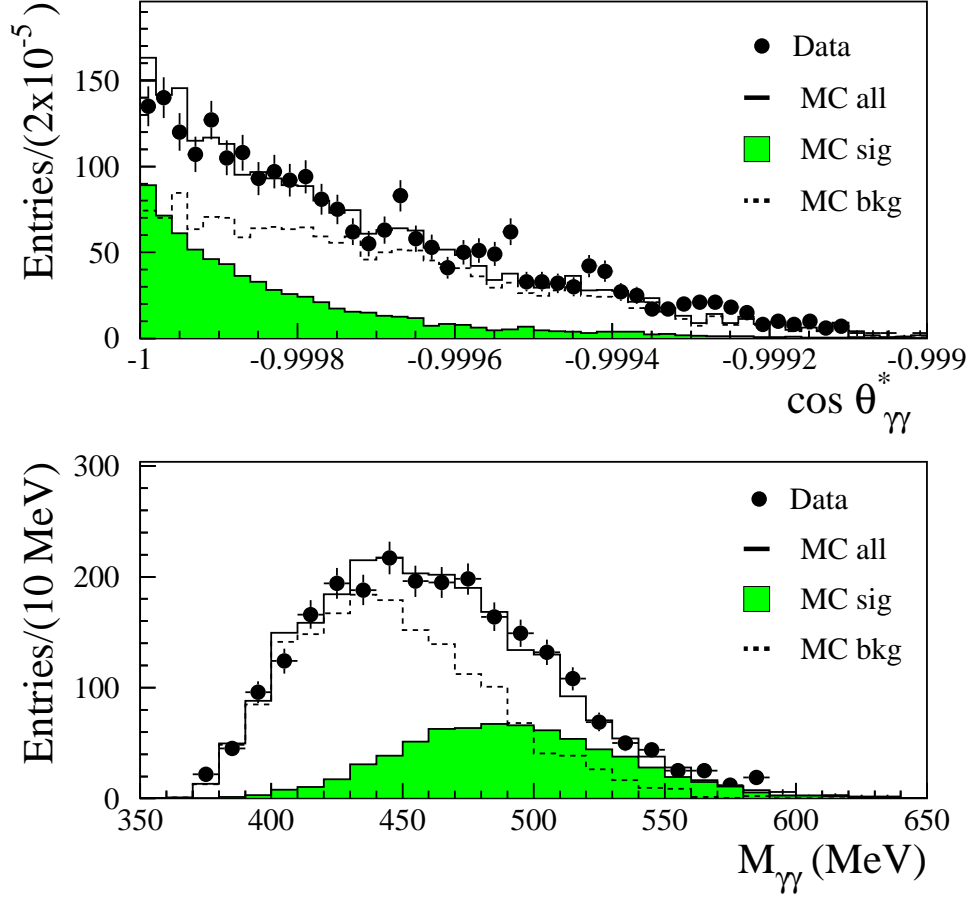


Figure 7: Distributions of $\cos(\theta_{\gamma\gamma}^*)$ (a) and $M_{\gamma\gamma}$ (b) for the final sample.

background-enriched samples obtained by requiring a complementary cut on χ^2 , such as $30 < \chi^2 < 500$. Moreover, to test the fit stability in different regions of the $M_{\gamma\gamma} - \cos \theta_{\gamma\gamma}^*$ plane, we have determined how much the result varies when: (1) reducing the fit-region along the $\cos \theta_{\gamma\gamma}^*$ axis or (2) fitting only in a signal dominated region shown by the ellipse in Fig. 4. The maximum variation of the BR for these tests is reported as background shape in Tab. 1.

We have also tested the stability of the branching ratio when modifying the width of the time window used for the QCAL veto from ± 5 ns to ± 4 , ± 6 ns. Similarly, the cut in χ^2 has been changed from 20 to 16 and 24. We have then repeated the fit by applying to the MC an energy-scale correction of +0.4%, a factor of two larger than what measured with the $K_L \rightarrow \gamma\gamma$ control sample. We have also checked that regrouping the bins of the 2-D plot by factors from 2 to 5 does not modify substantially the result. For all of these cases, the maximum variation of the BR obtained is used as systematic error and shown

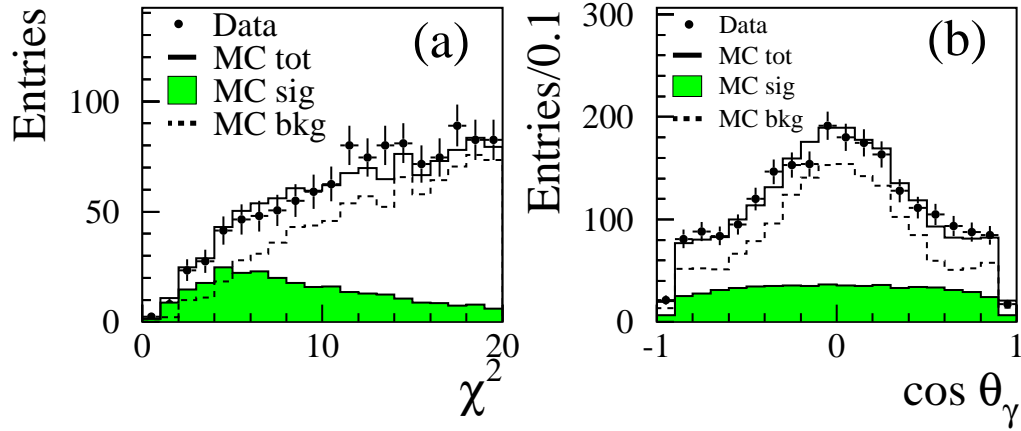


Figure 8: Distributions of χ^2 (a) and inclusive $\cos \theta_\gamma$ of the two photons in the event (b) for the final sample.

Source	$+\Delta\text{BR}/\text{BR} \text{ (\%)}$	$-\Delta\text{BR}/\text{BR} \text{ (\%)}$
Trigger, Filter, Tag	0.03	0.03
Signal acceptance	0.17	0.17
QCAL veto	0.02	0.26
χ^2 scale	1.80	1.80
Background shape	1.04	0.98
QCAL TW change	0.53	0.49
χ^2 change	0.99	—
MC Energy scale	—	0.79
2D-Fit binning	0.96	0.98
Normalization sample	0.15	0.15
Total	2.56	2.48

Table 1: Breakdown of the contributions to the total systematic error for the $\text{BR}(K_S \rightarrow \gamma\gamma)$.

in Tab. 1. The sum in quadrature of all entries is used as total systematic error.

For the normalization we count $K_S \rightarrow 2\pi^0$ tagged events with four prompt photons. An efficiency of

$$\epsilon_{sel}(2\pi^0) = (65.0 \pm 0.2_{\text{stat}} \pm 0.1_{\text{syst}})\% \quad (4.5)$$

is found by MC. As for the signal, the systematic uncertainty related to the cluster detection efficiency is evaluated by varying the data-MC correction curves. After correcting for $\epsilon_{sel}(2\pi^0)$, a number of $(190.5 \pm 0.2) \times 10^6$ $K_S \rightarrow 2\pi^0$ tagged events is obtained. The systematic uncertainty related to the presence of machine background clusters, fragmentation and merging of clusters is estimated by repeating the measurement in an inclusive way and counting tagged events with 3, 4 and 5 photons. The overall systematic error for

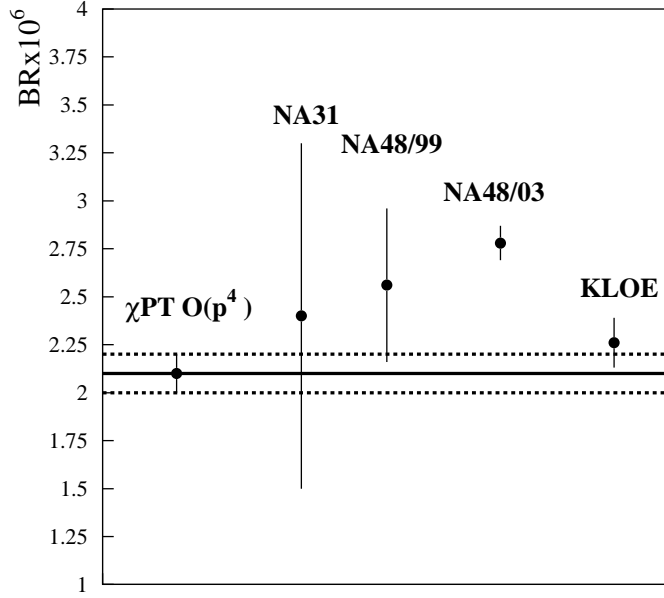


Figure 9: Comparison of our measurement of $\text{BR}(K_S \rightarrow \gamma\gamma)$ with the other existing measurements and $\mathcal{O}(p^4)$ χ PT predictions (horizontal band).

the normalization sample is reported in Tab. 1.

To evaluate $\text{BR}(K_S \rightarrow \gamma\gamma)$ we use the latest PDG [12] value $\text{BR}(K_S \rightarrow 2\pi^0) = (30.69 \pm 0.05)\%$. We obtain:

$$\text{BR}(K_S \rightarrow \gamma\gamma) = (2.26 \pm 0.12_{\text{stat}} \pm 0.06_{\text{syst}}) \times 10^{-6}. \quad (4.6)$$

We have repeated the measurement by subdividing the data in two sets to check stability for the slightly different running conditions: 1) 0.4 fb^{-1} from 2001-2002 and 2) 1.5 fb^{-1} for 2004-2005. Also the simulation has been divided accordingly. We get $\text{BR}(K_S \rightarrow \gamma\gamma) = (2.24 \pm 0.30_{\text{stat}}) \times 10^{-6}$ in 2001-2002 and $\text{BR}(K_S \rightarrow \gamma\gamma) = (2.26 \pm 0.13_{\text{stat}}) \times 10^{-6}$ in 2004-2005, which are in excellent agreement.

Comparison of our result with other existing measurements and $\mathcal{O}(p^4)$ χ PT theoretical predictions is shown in Fig. 9. There is a 3σ 's discrepancy between the present result and the measurement of NA48.

5. Conclusion

From ~ 2 billion ϕ mesons collected with KLOE at DAΦNE, we have measured the $\text{BR}(K_S \rightarrow \gamma\gamma)$ with a 5.3% statistical uncertainty and a $\sim 2\%$ systematic error. We obtain a BR result which deviates by 3σ 's from the previous best determination. Precise

χPT theory calculation for this decay are done at $\mathcal{O}(p^4)$. Higher order effects are predicted to be at most of the order of $\sim 20\%$ of the $\mathcal{O}(p^4)$ decay amplitude. Our measurement is consistent with negligible higher order corrections.

6. Acknowledgements

We thank the DAΦNE team for their efforts in maintaining low background running conditions and their collaboration during all data-taking. We want to thank our technical staff: G.F.Fortugno and F.Sborzacchi for their dedicated work to ensure an efficient operation of the KLOE Computing Center; M.Anelli for his continuous support to the gas system and the safety of the detector; A.Balla, M.Gatta, G.Corradi and G.Papalino for the maintenance of the electronics; M.Santoni, G.Paoluzzi and R.Rosellini for the general support to the detector; C.Piscitelli for his help during major maintenance periods. This work was supported in part by EUROPAPHNE, contract FMRX-CT98-0169; by the German Federal Ministry of Education and Research (BMBF) contract 06-KA-957; by the German Research Foundation (DFG), 'Emmy Noether Programme', contracts DE839/1-4; by DOE grant DE-FG-02-97ER41027; and by the EU Integrated Infrastructure Initiative HadronPhysics Project under contract number RII3-CT-2004-506078.

References

- [1] G. D'Ambrosio, D. Espriu, Phys. Lett. **B 175** (1986), 237.
J.L. Goity, Z. Phys. **C 34** (1987), 341.
F. Buccella, G. D'Ambrosio and M. Miragliuolo Il Nuovo Cimento **A 104** (1991), 777.
J. Kambor and B.R. Holstein, Phys. Rev. **D 49** (1994), 2346.
- [2] G. D. Barr, *et al.*, Phys. Lett. **B 351** (1995), 579.
- [3] A. Lai, *et al.*, Phys. Lett. **B 493** (2000), 29.
- [4] A. Lai, *et al.*, Phys. Lett. **B551** (2003).
- [5] KLOE collaboration, LNF-92/019(IR) (1992) and LNF-93/002(IR) (1993).
- [6] S. Guiducci, in: P. Lucas, S. Weber (Eds.), Proceedings of the 2001 Particle Accelerator Conference, Chicago, IL, USA, 2001.
- [7] KLOE collaboration, M. Adinolfi *et al.*, Nucl. Inst. Meth. A 488 (2002), 51.
- [8] KLOE collaboration, M. Adinolfi *et al.*, Nucl. Inst. Meth. A 482 (2002), 364.
- [9] KLOE collaboration, M. Adinolfi *et al.*, Nucl. Inst. Meth. A 483 (2002), 649.
- [10] KLOE collaboration, M. Adinolfi *et al.*, Nucl. Inst. Meth. A 492 (2002), 134.
- [11] KLOE collaboration, F. Ambrosino *et al.*, Nucl. Inst. Meth. A 534 (2004), 403.
- [12] W.M.Yao *et al.*, Journal of Physics G 33, (2006), 1.

